A Multiscale Coarse-Graining Study of the Liquid/Vacuum Interface of Room-Temperature Ionic Liquids with Alkyl Substituents of Different Lengths

Wei Jiang,[†] Yanting Wang,[†] Tianying Yan,[‡] and Gregory. A. Voth*,[†]

Center for Biophysical Modeling and Simulation and Department of Chemistry, University of Utah, Salt Lake City, Utah 84112-0850, and Institute of New Energy Material Chemistry, Nankai University, Tianjin 300071, China

Received: September 23, 2007

Multiscale coarse-grained (MS-CG) molecular dynamics simulations were performed for the liquid−vacuum interface of room-temperature ionic liquids having alkyl substituents of different lengths. Surface properties, such as the number density profile, the orientational ordering, and surface tension, were calculated. Both CG site and electron number density profiles show that, for the ionic liquids with a long enough alkyl chain, a unique multilayer ordering occurs. In contrast, ionic liquids with a shorter chain exhibit an interfacial structure consistent with a monolayer ordering. Detailed analysis indicates that such mono/multilayer ordering results from the strong electrostatic interactions among the polar groups, and the collective short-range interactions among the nonpolar groups. Such surface behavior may be interpreted as the two-dimensional manifestation of bulk spatial heterogeneity in ionic liquids (Wang, Y.; Voth, G. A. *J. Am. Chem. Soc.* **2005**, *127*, 12192). The orientational behavior of the cation shows that the alkyl chain tends to align parallel to the surface normal, while the aromatic ring is preferentially perpendicular to the surface normal for all the underlying species. An analysis for the surface electron density demonstrates that the cation plays a key role in determining the surface electron density oscillations, while the anion only marginally affects the enhancement. The surface tension is seen to monotonically decrease and approaches a constant as the chain length increases, in agreement with Langmuir theory and experiments.

I. Introduction

Room-temperature ionic liquids (ILs) have generated considerable interest both theoretically and experimentally, since they are potential replacements for traditional solvents used in chemical processes.[1−3] An IL is a salt composed of an asymmetric organic cation and, most commonly, an inorganic anion, which is at or near room temperature. These solvents have the ability to dissolve a range of inorganic, organic, and polymetric materials at very high concentrations. They are noncorrosive with low viscosities and no significant vapor pressure.[4−6] Other features, such as reusability, better reactivity, and selectivity, also suggest that ILs may be good candidates for "green chemistry".

A rapidly developing application area for ILs are two-phase homogeneous catalytic reactions.[7,8] Such catalytic processes are believed to occur at the interface of the ILs and a given organic liquid. The rate of the chemical reaction depends on the ability of the catalyst to access the surface and the permeation of material across the interface. The structure and dynamics of their vapor/liquid interface is therefore one of the central concerns. Recently, the structure of the vacuum/IL interface has been investigated computationally[9−13] and experimentally.[14−25] Most of these studies focus on 1-alkyl-3-methylimidazolium-based ILs. Molecular dynamics (MD) simulations for the vacuum/liquid interface of ILs of dialkylimidazolium ($DMIM^+$) cation and various anions show that the N−N bond of the aromatic ring tends to point to the surface with the terminal methyl group on the alkyl chain protruding from the surface. There is also a region of enhanced number density, in which the vertical alignment of the molecular planes allows the cation to pack more closely. Recent MD simulations[10,12,13] also present a similar monolayer-ordering interfacial structure for the $BMIM^+/PF_6^-$, $BMIM^+/BF_4^-$, and $EMIM^+/NO_3^-$ ILs.

Bowers and Vergara-Gutierrez[21] used neutron reflectometry (NR) to probe the interfacial structure of the ILs 1-butyl-3-methylimidazolium tetrafluoroborate ($BMIM^+/BF_4^-$) and 1-octyl-3-methylimidazolium hexafluorophosphate ($OMIM^+/PF_6^-$). Their results suggest that the cationic head groups and anions are segregated from the alkyl-rich region and with a stratified structure that exists with at least two tiers of alkyl groups. An electron density oscillation near the surface is also evident from this study, and so it was supposed that a multilayer ordering occurs. Gannon et al.[14] performed the first direct recoil spectrometry (DRS) to investigate the molecular composition and orientation at the surface of the 1-butyl-3-methylimidazolium hexafluorophosphate ($BMIM^+/PF_6^-$) system. They found that the number of cations and anions is nearly equal at the surface and, statistically, that the cations tend to lie normal to the liquid surface while the terminal C2 site points out toward the gas phase. Law and Watson[15] performed a systematic investigation of the surface tension of *N*-alkyl-imidazolium ILs employing a conventional ring tensiometer. They found that the surface free energy always decreases with increasing length of the alkyl chain in the 1-position. Baldelli and Rivera-Rubero[18,20] performed sum frequency generation (SFG) spectroscopy on the 1-butyl-3-methylimidazolium bisperfluoralkylimide ILs, and their study indicated that the butyl group chains protrude out

* Author to whom correspondence should be addressed. E-mail: voth@chem.utah.edu.
[†] University of Utah.
[‡] Nankai University.

10.1021/jp077643m CCC: $40.75
Published on Web 01/05/2008

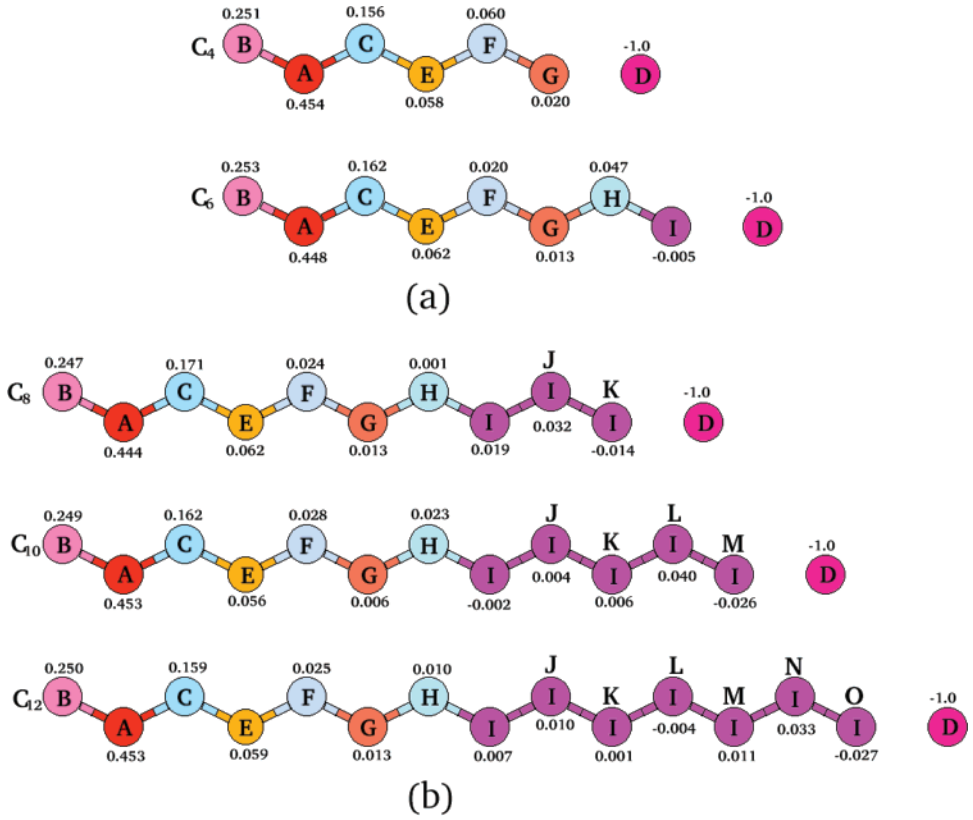

Figure 1. CG models of ILs used in the present paper: (a) The CG models for C_4 and C_6; (b) the CG models for C_8, C_{10}, and C_{12}. Site A represents the aromatic ring of the cation (head), and site D represents the anion. Site B represents the methyl group bonded to the head. For C_4 and C_6, the sites G and I represent the tail groups (CH3−), while the other sites represent the methylene groups (−CH2−). For C_8, C_{10}, and C_{12}, the extended sites I demonstrate that they share the same nonbonded force field as the site I in C_6. The letters outside the sites represent their actual labels used in the subsequent plots and MD simulations. The numbers on the sites are their partial charges.

of the interface into the vacuum. They also suggested that the cation is likely to be segregated on the surface. Limori et al.[22] further reported that similar interfacial structure exists for IL species with longer alkyl chains. Solutskin et al.[23] performed an X-ray reflectivity (XR) on $BMIM^+/(PF_6^-$ and $BF_4^-)$. They also found an electron density enhancement. However, none of the three possible molecular arrangements they suggested is in accordance with the other existing results. More interestingly, recently Halka and co-workers[24,25] have reported an order−disorder interfacial phase transition phenomenon.

Despite the extensive experimental and computational studies in the past few years, the current body of knowledge of the surface properties of ILs still seems insufficient, with an understanding of the IL/vacuum interface based mainly on the short alkyl-chain species. The surface properties of the long alkyl-chain ILs as well as their intrinsic connection with the short alkyl-chain species remains to be explored. One of the main difficulties is that any reliable IL MD simulation usually requires at least hundreds of molecules ($\sim 10^4-10^5$ atoms). In addition, the interface simulation requires a larger system size than the bulk to eliminate the finite size effect and very long simulation times to properly equilibrate the system. Thus, all-atom MD simulations of many IL interfaces are very demanding and even infeasible.

Recently, a "multiscale coarse-graining" (MS-CG)[26−28] approach based on the force-matching (FM) method has been developed. The MS-CG approach calculates the effective pairwise force field between CG sites systematically from an underlying explicit atomistic MD simulation by force-matching the coarse-grained image of atomistic trajectory and force data. The radial distance between pairwise CG sites is divided into bins, and the force inside each bin is fitted individually. The force fields so-obtained are tabulated and no longer restricted to a simple analytical form for the range of its radial distance. It has been shown that the MS-CG models can easily simulate a bulk system ten to hundreds of times larger than the polarizable atomistic MD model for ILs for a given amount of CPU time.[27]

In this study, we report MS-CG MD simulations of the liquid/vacuum interface of IL species with various side-chain lengths to provide a clearer picture of IL−vacuum interface properties. In our previous work,[27] an MS-CG model for $EMIM^+/NO_3^-$ was successfully developed, which gives good agreement with the structural and thermodynamic properties of an atomistic polarizable MD IL model.[29,30] This MS-CG model has also been extended to qualitatively investigate the spatial heterogeneity in ILs.[31] In the present work, an MS-CG procedure similar to that in refs 27 and 31 is applied to the longer-chain IL species to develop more accurate MS-CG models. The IL−vacuum interface MS-CG simulations are then performed using the new models.

The structure of this paper is as follows: In section II, the models and simulation methodology are described. Section III reports the simulation results and a discussion is given. Section IV provides concluding remarks.

II. Models and Simulation Methodology

A. The Atomistic Polarizable Model. For ILs, both simulations[32−35] and experiments[36,37] have found that the local environment around the IL ions is highly anisotropic. For such a system, it is desirable to model the ILs with an electronically polarizable model, which can model the electron density

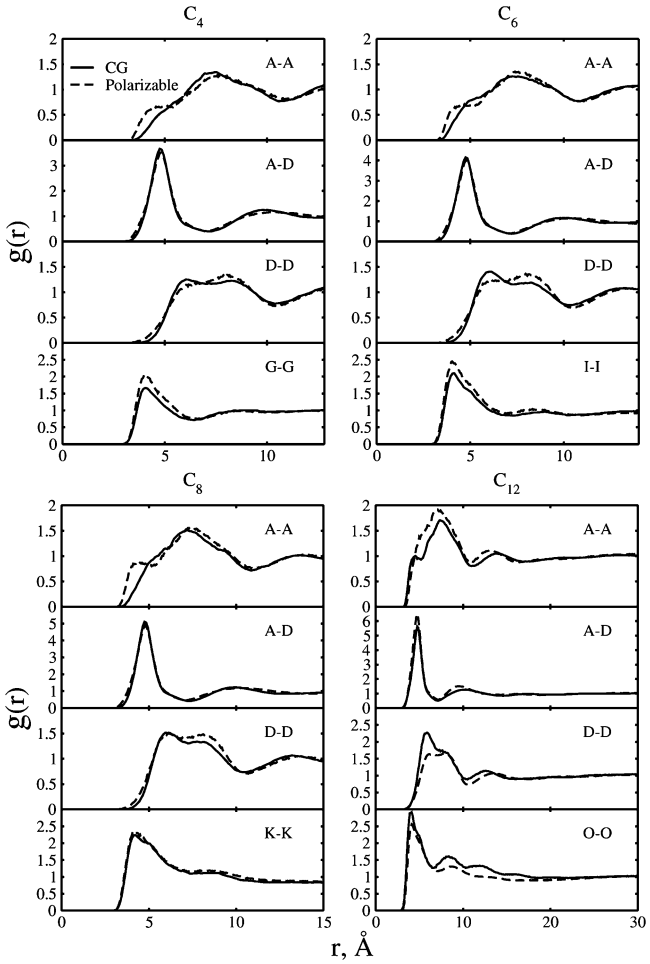

Figure 2. Selected site−site RDFs from the atomistic simulation (dashed lines) compared to those from the MS-CG MD simulation (solid lines), with the four RDFs head−head, head−anion, anion−anion, and tail−tail shown.

TABLE 1: Simulation Details of Different Systems

CG model	ion pairs	simulation cell size (X, Y, Z)	equilibration length (ns)	production length (ns)
C_4	686	46.3, 46.3,139 Å	1.0	4.0
C_6	686	49.2,49,2,147.6 Å	1.0	4.0
C_8	686	52.5,52.5,157.5 Å	1.0	4.0
C_{10}	1029	55.0.55.0,215.0 Å	1.5	5.5
C_{12}	1029	57.7,57.7,223.1 Å	1.5	5.0

distortions. Recently, Yan et al.[29] have developed a polarizable model for ILs, which relies on an extended Lagrangian approach, similar in spirit to the Car−Parrinello method.[38,39] Despite the increased simulation time, the polarization caused by the induced dipoles has been shown to have a significant influence on both the structural and the dynamical properties of ILs.[29] The polarizable model also brings the atomistic results into closer agreement with the experimental data.

The total potential energy of the polarizable model is given by

$$V_{\text{polar}} = V_{\text{bond}} + V_{\text{nonbond}} + V_{\text{ind}} \quad (1)$$

where the V_{bond}, V_{nonbond}, and V_{ind} are expressed, respectively, as

$$V_{\text{bond}} = \sum_{\text{bonds}} k_b(r - r_0)^2 + \sum_{\text{angle}} k_\theta(\theta - \theta_0)^2 + \sum_{\text{dihedrals}} V_n \cos(n\phi - \gamma) \quad (2)$$

$$V_{\text{nonbond}} = \sum_i \sum_{j>i} \left(\frac{a_{ij}}{r_{ij}^{12}} - \frac{b_{ij}}{r_{ij}^{6}} + \frac{q_i q_j}{r_{ij}} \right) \quad (3)$$

$$V_{\text{ind}} = -\sum_i \mu_i \cdot \mathbf{E}_i^0 - \sum_i \sum_{j>i} \mu_i \cdot \mathbf{T}_{ij} \cdot \mu_j + \sum_i \frac{\mu_i \cdot \mu_j}{2\alpha_i^2} \quad (4)$$

The term $V_{\text{bond}} + V_{\text{nonbond}}$ comprises the standard nonpolarizable model.

In the above equations, the force field parameters for the nonpolarizable model were provided in the standard Amber force field[40] and have been used in previous work.[12,29,41] The partial charges of both cations and anions were obtained by fitting the ab initio electrostatic potentials (ESP) with the RESP fitting package.[40] The ab initio calculations were performed with Gaussian 03.[42] The ESP grids were generated by the MP2/6-31G(d) level of theory and fit to the MP2/6-31G(d) optimized structure. The RESP partial charges are valid for both nonpolarizable and polarizable force field models. In V_{ind}, the first term represents charge−dipole interactions, the second term represents dipole−dipole interactions, and the last term is the energy required to induce the dipole. The term $\mathbf{E}_i$ is the electric field on atom i, generated by the partial charges of all other atoms, excluding those within the same ion of atom i. The dipole field tensor $\mathbf{T}_{ij}$ is calculated from the ESP $\phi^f(|\mathbf{r}_i - \mathbf{r}_j|)$ at point j due to the charge at point i: $\mathbf{T}_{ij} = \nabla_i \nabla_j \phi^f(|\mathbf{r}_i - \mathbf{r}_j|)$. The induced dipole moment is $\mu_i = \alpha_i[\mathbf{E}_i + \sum_{j=1,j\neq i}^{N} \mathbf{T}_{ij} \cdot \mu_j]$, where α_i is the isotropic atomic polarizability of atom i. The isotropic atomic polarizabilities were determined by fitting the anisotropic molecular polarizabilities of the ions, which can be obtained by an ab initio calculation.

B. CG Procedure. For convenience, the IL systems are denoted by the number of carbons on the alkyl chain, e.g., $BMIM^+/NO_3^-$ is denoted as C_4 and $HMIM^+/NO_3^-$ is denoted as C_6. In the same manner as in ref 27, the atoms for C_4 and C_6 were grouped into 7 and 9 CG sites, respectively. The resulting structures of the MS-CG models are shown in Figure 1a. The C_4 and C_6 systems composed of 64 ion pairs were equilibrated with polarizable atomistic models in the constant NPT ensemble by a Hoover barostat[43] at a temperature $T = 400$ K and a pressure $P = 1$ atm, with a time step of 0.45 fs. With the volume set to be the average volume obtained from the constant NPT run, the systems were then equilibrated again, using a constant NVT ensemble with a Nosé−Hoover thermostat[44] at $T = 400$ K until a constant diffusion coefficient was observed. After this equilibration stage, the simulations were further performed for an additional 5×10^6 MD time steps, and a trajectory of a total 2.25 ns in constant NVT ensemble was then produced. During the simulation, 5000 configurations were sampled at an interval of 1000 steps. For each configuration, the system virial, as well as the positions, velocities, and forces of all atoms, were recorded. The revised DL_POLY 2.13 package was used to implement the MD simulations for both the atomistic and MS-CG models.

With the partial charge of each CG site fixed (as the sum of the underlying atomistic partial charges), the FM and bonded parameter fitting procedures as described in ref 27 were applied to the 5000 configurations to find the best fit for both the short-range nonbonded forces and the intramolecular force field parameters.

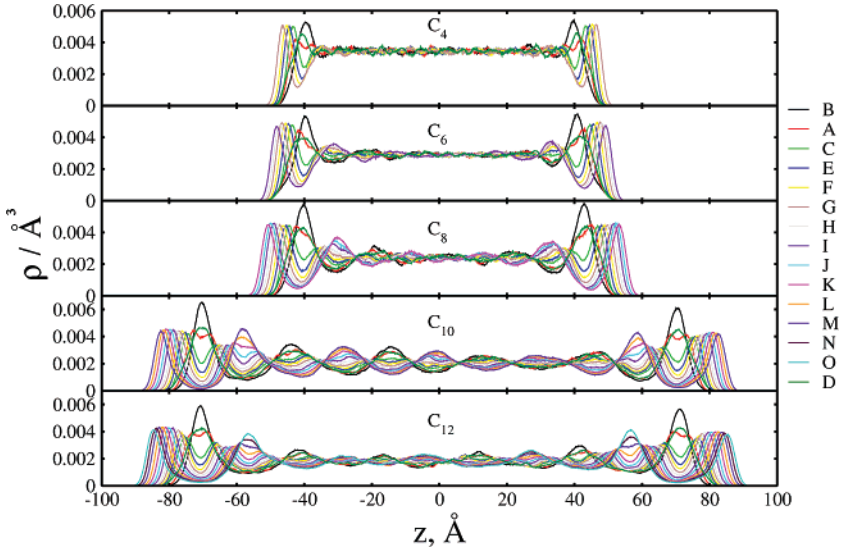

Figure 3. CG site surface normal DPFs from C_4 to C_{12}.

The MS-CG model of C_6 was then extended with more I sites to form C_8, C_{10}, and C_{12}, respectively, with the partial charges fixed in the same manner as C_4 and C_6. The MS-CG models for these systems are shown in Figure 1b.

In Figure 2, the four most representative CG site−site distribution functions of C_4, C_6, C_8, and C_{12} are compared with their corresponding atomistic MD radial distribution functions (RDFs), indicating that not only the fitted bonded and matched nonbonded MS-CG force fields are able to reproduce the IL structural properties accurately for C_4 and C_6, but also the extended MS-CG models are quantitatively reasonable.

C. MD Simulation Methodology for the CG Models. As the cationic side-chain length increases, the number of CG sites increases with the given number of ion pairs. For the interfacial simulations, systems with longer alkyl chains may have a more significant finite size effect in a finite simulation box that is big enough for systems with shorter chains. However, obtaining fully equilibrated IL systems with a large enough simulation size is not easily done. In this study, an equilibration strategy aimed to accelerate the equilibration in the MD simulations was performed and consists of three distinct steps: In step 1, an initial configuration containing 343 ion pairs was manually constructed, with the ions positioned on the select lattice positions within a large cubic simulation box. The initial configuration was then equilibrated at $T = 400$ K with a constant NPT simulation for 1 ns. The final configuration at $T = 400$ K was then re-equilibrated under constant NVT conditions, as done previously. In step 2, the fully equilibrated configuration with 343 ion pairs was duplicated once in the *z*-direction for C_4, C_6, and C_8 to obtain an initial configuration with 686 ion pairs; for C_{10} and C_{12}, the configuration was duplicated twice to obtain an initial configuration with 1029 ion pairs. The new configurations with either 686 or 1029 ion pairs were equilibrated at 1000 K under constant NVT conditions. The final configuration at 1000 K was then cooled down sequentially to 400 K, at intervals of 200 K. At each different temperature, the system was equilibrated for 500 ps, adding up to a total pre-equilibration run of 2 ns. In step 3, the pre-equilibrated configuration was then placed at the center of a larger supercell with elongated *z*-cell length and the same *x*,*y* cell dimensions. The result is two equivalent IL−vacuum interfaces within a single supercell. MD simulations were then performed on these generated by the planar IL slabs in a constant NVT ensemble at 400 K. In all the simulations, the supercell was set up using three-dimensional rectangular boundary conditions. The distance between two neighboring slabs is set to be 50 Å to eliminate the long-range interaction between them. The parameters for these simulations are summarized in Table 1. The choice of the supercell sizes is aimed to keep a well-stabilized bulk-like region in the middle of the system as well to prevent the two

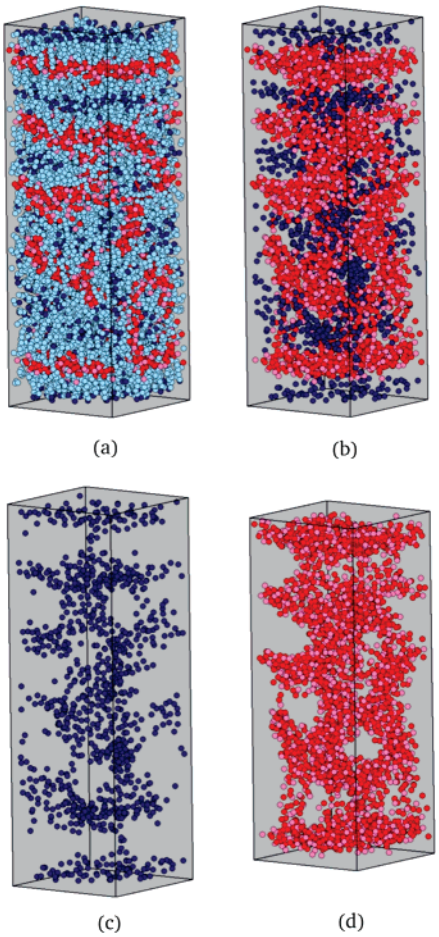

Figure 4. A snapshot for C_{12} at the end of the MD trajectory data: (a) all CG sites are shown; (b) the sites A, D, and O are shown; (c) the sites A and D are shown; (d) the sites O are shown. The head groups (sites B have been put into the head groups for convenience), D, O, and all the other sites on the side chain are colored red, purple, dark blue, and light blue, respectively.

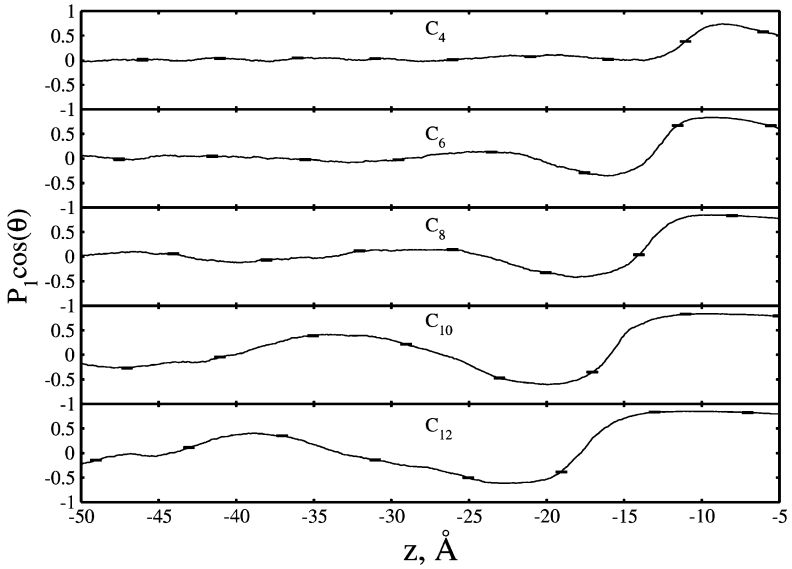

Figure 5. Orientational ordering of the various cations at the interface. The cosine of the angle between the alkyl chain vector and the surface normal as a function of the height related to the interface is reported. The chain vector is defined as the vector pointing from the head to the alkyl terminal site. The ordering parameter was calculated by a histogram method with a bin width 0.1 Å. The existence of a head group depletion region at the interface causes poor statistics; therefore the outer 5 Å along the surface normal was removed for each panel.

equivalent interfaces from interacting with each other. The integration time step was 1.0 fs, and after the equilibration run of the simulation, configurations from the MD trajectory were stored every 0.1 ps during the production run. No detectable vaporization was observed during the simulation.

III. Results and Discussions

A. CG Site Number Density Profile. Figure 3 shows the CG site number density profiles (DPFs) for IL species of various alkyl chains with the same anion, NO_3^-. The surface layering phenomena can be seen for all of the species. The surface normal inhomogeneity extension ranges tens of angstroms as the side-chain length increases, and is accompanied by stronger and stronger surface number density enhancement. More impressively, from C_6 onward, a multilayer ordering occurs with a decaying DPF that extends into the bulk.

A common feature in these DPFs is the microscopic phase separation between the polar groups (head-groups and the anions) and nonpolar groups (alkyl tail) at the interface. For example, within the surface monolayer of C_4, the methyl and polar groups (CG sites B, A, and D) tend to be located at the bulk side, while the butyl groups are on the vacuum side. For each $BMIM^+$ at the interface, the butyl group has a strong tendency to lie upright. This result is consistent with the atomistic level observations by Lynden-Bell and Del Popolo[10] for C_4.

To better understand the interfacial microscopic phase separation, a snapshot of C_{12} from the MD trajectory data is shown in Figure 4. Figure 4a demonstrates that the polar and nonpolar groups form separated heterogeneous structures in the bulk, as observed by Wang et al.[31,41] and Lopes and Pádua.[45] At the interface, the nonpolar and polar groups form their own respective domain layers, with the alkyl chains protruding. A clearer phase separation picture is shown in Figure 4b, where it can be seen that the head groups and the alkyl terminal sites form an even more prominent separation. As the phase separation extends to the surface, the polar groups form a domain layer under the alkyl-rich layer, in which each site is progressively nearer to the vacuum side from the methyl group to the alkyl terminal site within each cation (Figure 3). Therefore, the surface layering of ILs may be explained as a two-dimensional sub-representation of the three-dimensional microscopic phase separation.

A more physical explanation of the phenomena described above is as follows: For the polar groups, the hydrogen bond interactions, which have been force-matched into a short-range force, as well as the strong Coulomb interactions, make the anions and the head groups always form a stable local structure for various side-chain lengths, as indicated by the single sharp peak in the A−D RDFs of Figure 2. Globally, these interactions make the polar group form a continuous three-dimensional network in the bulk and the nonpolar groups permeate the polar network. Therefore, both the nonpolar and polar groups form their own three-dimensional heterogeneous structures. Figure 4c shows only the heterogeneous distribution of terminal sites of the alkyl chain for clearer identification, and Figure 4d demonstrates the heterogeneous network formed by the charged polar groups. At the two-dimensional liquid/vacuum interface, however, besides the mechanism mentioned above, the collective van der Waals interactions of nonpolar groups make them result in a lower energy surface than that of the charged polar groups. As a result, the nonpolar groups segregate to the vacuum side, while the polar groups protrude into the bulk, forming a typical Langmuir monolayer at the interface. Additionally, the intramolecular interactions lead to the observed progressive alignment of the sites within each cation.

In addition, from C_6 onward, the large surface normal inhomogeneity extension in the top layer forms an obvious multilayer ordering. As previously mentioned, the phase separation exists in the whole system, and in the sub-space just below the top layer it inevitably "feels" the geometrical influence from the top layer. As a result, just below the top layer, there are additional narrower layers. Between any two neighboring layers, the phase of the respective site number density oscillation is always opposite to each other, in accordance with the microscopic phase separation. This indirect dimensionality effect is more significant as the alkyl chain length (asymmetry) increases. It can also be noticed that, in C_{10} and C_{12}, strong density oscillations persist into the bulk. Compared with C_6 and C_8, such a non-vanishing density oscillation can be attributed to

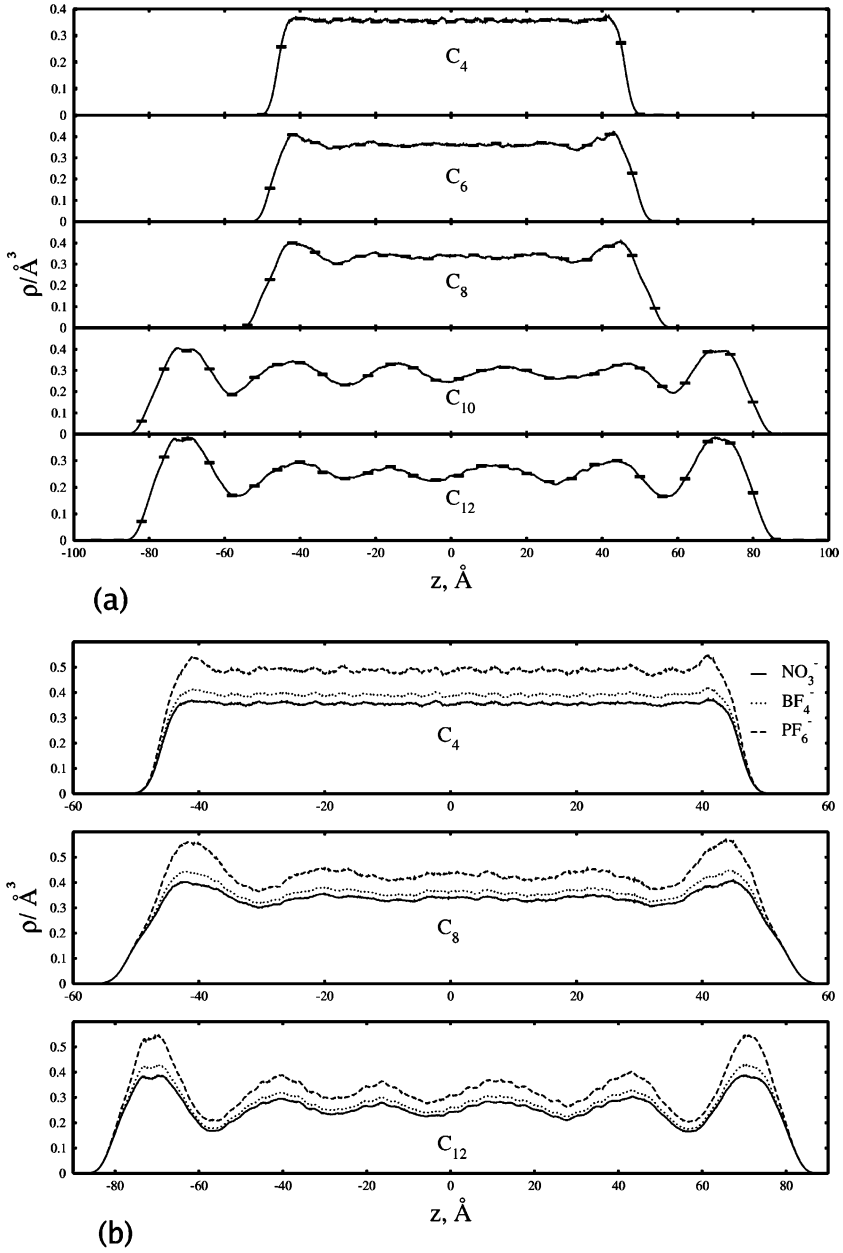

Figure 6. Electron DPFs from C_4 to C_{12}: (a) various cations with the same anion NO_3^-; (b) for C_4, C_8, and C_{12}, with three types of anions as shown.

the much larger characteristic length scale of nanostructural organization than in the liquid bulk. As a result, within the time scale of the MD simulation, the strong heterogeneity in the bulk part of the simulation cell cannot be effectively averaged out, even with the MS-CG models being used.

B. Orientational Ordering. Figure 5 shows the orientation ordering of the alkyl chains at the interface. In accordance with the progressive alignment of the cation sites in Figure 3, the alkyl chain is shown to be preferentially aligned parallel to the surface normal, with the angle between the chain vector and the surface normal approaching ∼30° for C_{10} and C_{12}. Another prominent feature is that the interfacial alkyl orientation zone becomes broader and broader as the chain length increases, with the width of the interfacial orientation zone being ∼3 Å for C_4, ∼8 Å for C_6 and C_8, and ∼15 Å for C_{10} and C_{12}. This trend follows along with the augmentation of surface layering. In Figure 3, it can be seen that the number density enhancement of the top layer related to the bulk gradually rises from ∼45% to ∼100%; on the other side, the top layer width increases simultaneously, resulting in a broader and broader orientation zone.

An additional ordering parameter is the orientation behavior of the aromatic ring. In both Yan et al.'s[12] and Lynden-Bell et al.'s[10,11] work, the interfacial orientation behavior of the aromatic ring for the short-chain species was examined within ring sizes that were similar to the alkyl chain. In the present MS-CG models, however, the cation ring has been coarse-grained into a single site, so calculating the ring orientation is not straightforward as in the full-atom simulations. Rather, it had to be inferred from the two adjacent sites connected to the ring. Previous MD simulation and ab initio calculations demonstrate that the two adjacent C−N bonds are almost located in the same plane as the ring; the present MS-CG models can therefore use the A−B and A−C bonds as an approximate representation. As shown in Figure 3, it is observed that along the surface normal, the sites B, A, and C are progressively separated by

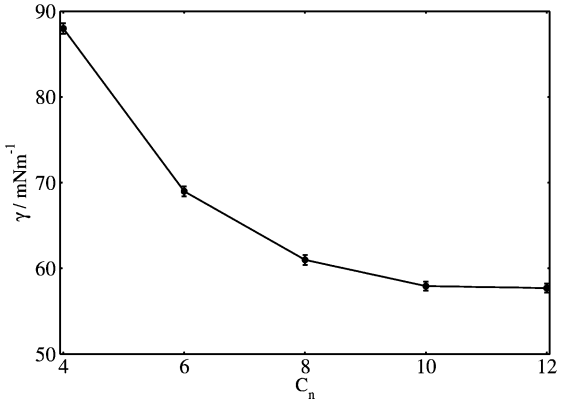

Figure 7. Surface tensions for C_4 to C_{12}. The horizontal axis is the number of the carbon atoms on the side chain. The values shown, from C_4 to C_{12}, are 88.04 ± 0.61, 69.1 ± 0.58, 61.04 ± 0.59, 57.94 ± 0.52, and 57.71 ± 0.53 mN m^{-1}, respectively.

∼2.5 Å, close to the fitted A−B and A−C bond lengths. It can be thus *qualitatively* concluded that the ring normal tends to be perpendicular to the surface normal for all the species. This tendency is consistent with the compact packing of the alkyl chains closer to the vacuum, as well as with experiment.[14,17]

C. Electron DPF. Figure 6a shows the surface normal electron DPFs from C_4 to C_{12} with the anion NO_3^-. For C_4, the profile demonstrates that there is no electron density oscillation and only a small (∼3%) density enhancement at the interface. From C_6, corresponding to Figure 3, the electron density shows obvious oscillations extending into the bulk and an enhancement at the interface. This result is in good agreement with the experimental observation of Bower et al.[21] On the basis of the multilayer ordering phenomena, the physical interpretation of the electron density oscillation is straightforward: an alkyl rich region is located on top of a region consisting of the headgroups and the anions, which is, in turn, on top of an inner alkyl-rich layer.

For a better comparison with the relevant experimental results and to more accurately investigate the roles that the cation and anion play in affecting the surface normal electron density, the electron number of NO_3^- was replaced by that of BF_4^- and PF_6^-, respectively, with the same trajectory data used. This replacement can be justified by the packing behavior of the anion, the aromatic ring is mainly determined by the strong electrostatic attraction, and, in general, different anions can only cause subtle difference given the same imidazolium-based cation, as shown in many IL simulations.[45−48] Figure 6b shows the electron DPFs for C_4, C_8, and C_{12} with the three types of anions. For C_4, the electron density still does not show any oscillation at the interface, but the enhancement becomes distinct as the electron number of the anion increases. For PF_6^-, the interfacial sharp peak is ∼10−15% higher related to the bulk, which is consistent with the experiment.[23] For BF_4^-, the enhancement is ∼5%. For C_8 and C_{12}, the electron density shows the same oscillation behavior, though the interfacial enhancement is much different due to different anions.

From the above results, a systematic conclusion for the electron density behavior resulting from different cations and anions can be provided: The cation exclusively controls the electron density oscillation for any species, while, for the species before C_6, the anion determines the enhancement at the interface; for the species from C_6 and beyond, both the cation and anion contribute to the enhancement.

D. Surface Tension. Figure 7 shows the surface tensions from C_4 to C_{12}. It can be observed that the surface tension decreases as the alkyl chain length increases. From C_4 to C_8, the surface tension curve descends rapidly and then tends to approach a constant value from C_{10} onward. Such a trend is in good agreement with the Langmuir principle,[49] as well as with experiment.[15,50] The Langmuir principle states[49] that, "each part of a molecule possesses a local surface free energy and the measured surface tension should correspond to the part of the molecule that is actually present at the interface". In Figures 3, 4, and 5, it can be clearly observed that the alkyl tail plays a significant role in determining the surface structures due to the two-dimensional microscopic phase separation. Correspondingly, the polarity of the surface is weaker and weaker, causing the surface tension to decrease. It is natural to consider that, with a species having a long enough alkyl tail, where the polar groups are far enough away from the surface, the surface will be nonpolar, and its stability is controlled by the mixing of the outer most methylene and methyl groups. It is likely that C_{12} has played the role of such a species from our simulations.

One problem with the above discussion is that our surface tension calculation is *semiquantitative*. Note that each value in Figure 7 is ∼150% larger than the corresponding experimental value.[15,50] This effect can be attributed to the MS-CG methodology: the CG scheme cannot completely capture the permanent dipole interaction that is modeled with the all-atom model. The

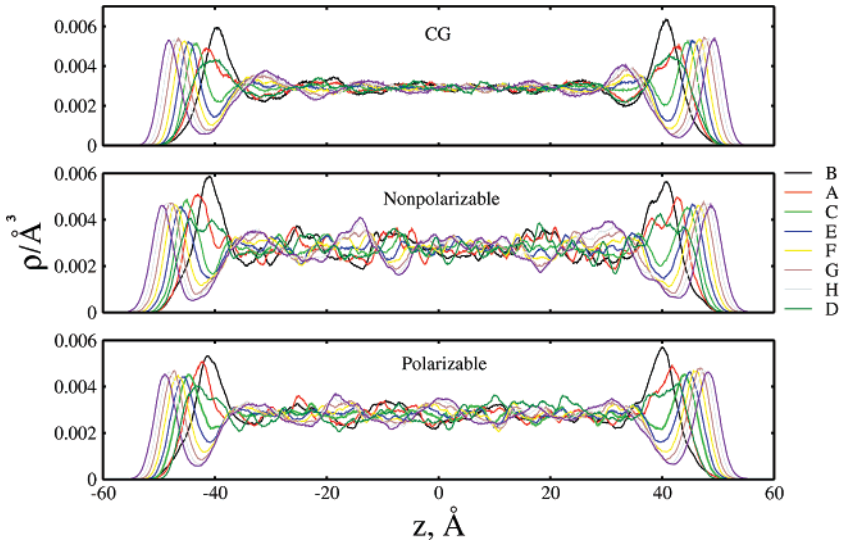

Figure 8. A comparison of the surface normal DPFs of C_6 for MS-CG and all-atom nonpolarizable and polarizable models.

MS-CG force field is fitted in the bulk, where the virial of the atomistic system can be well defined; however, the virial at the interface cannot be so easily controlled. Finding solutions for these problems is a topic for future research.

E. Comparison between MS-CG and Atomistic Simulations. To compare the accuracy of MS-CG simulations with the corresponding atomistic ones for IL species with a longer side chain than C_4, MD simulations with both all-atom polarizable and nonpolarizable models were performed for the C_6/vacuum interface system, under the same conditions as the corresponding CG supercell. The trajectory data were taken from a 2.25 and 3.0 ns production run after a 1 ns pre-equilibration run, for the polarizable and nonpolarizable models, respectively. These two tentative atomistic simulations cost nearly 90000 CPU hours on a Dell Dual-Core Linux Cluster, relative to ∼2600 CPU hours for the corresponding MS-CG simulation. Figure 8 shows the surface normal DPFs obtained from the MS-CG and all-atom nonpolarizable and polarizable MD simulations, respectively. It can be seen that the structure of outermost monolayer obtained from the MS-CG simulation agrees well with the atomistic simulations. However, below the outermost monolayer, the DPFs of atomistic simulations look so jagged that no clear picture of layering can be observed. However, the dynamics of an all-atom system is at least one order slower than the corresponding MS-CG one; especially in the present case, an all-atom simulation tends to be trapped into local minima of the potential surface due to the complex molecule packing/aggregation behavior below the monolayer.

III. Concluding Remarks

In this paper, a set of MS-CG models were developed for the 1-alkyl-3-methylimidazolium-based ILs with alkyl substituents of different lengths. The MS-CG MD simulations for the liquid/vacuum interface of these ILs were then carried out. The results provide a comprehensive picture for the IL/vacuum interface structure. As the side chain length increases, an evolution from monolayer to multilayer ordering was observed, resulting in the phenomenon of surface electron density oscillation, in agreement with experiment. The orientational behavior of the cation along the surface normal was seen to result from the formation of an outermost Langmuir monolayer, which also causes the surface tension to decrease monotonically and approach a constant value from C_{10} onward, again in agreement with the experiment.

Acknowledgment. This research was supported by Air Force Office of Scientific Research. The authors thank Dr. Gary Ayton and Dr. Pu Liu for valuable discussions. Computations in this research were supported in part by a challenge grant from the Department of Defense High Performance Computing Modernization Office.

References and Notes

(1) Rogers, R. D.; Seddon, K. R. *Science* **2003**, *302*, 792.
(2) Wasserscheid, P.; Keim, W. *Angew. Chem., Int. Ed.* **2000**, *39*, 3772.
(3) Welton, T. *Chem. Rev.* **1999**, *99*, 2071.
(4) Gordon, C. M.; Holbrey, J. D.; Kennedy, A. R.; Seddon, K. R. *J. Mater. Chem.* **1998**, *8*, 2627.
(5) Hagiwara, R.; Ito, Y. J. *Fluorine Chem.* **2000**, *105*, 221.
(6) Holbrey, J. D.; Seddon, K. R. *J. Chem. Soc., Dalton Trans.* **1999**, 2133.
(7) Olivier, H.; Chauvin, Y. *Chem. Ind.* **1996**, *68*, 249.
(8) Chauvin, Y.; Olivier-Bourbigou, H. *CHEMTECH* **1995**, *25* (9), 26.
(9) Lynden-Bell, R. M. *Mol. Phys.* **2003**, *101*, 2625.
(10) Lynden-Bell, R. M.; Del Popolo, M. G. *Phys. Chem. Chem. Phys.* **2006**, *8*, 949.
(11) Lynden-Bell, R. M.; Kohanoff, J.; Del Popolo, M. G. *Faraday Discuss.* **2005**, *129*, 57.
(12) Yan, T.; Li, S.; Jiang, W.; Gao, X.; Xiang, B.; Voth, G. A. *J. Phys. Chem. B.* **2006**, *110*, 1800.
(13) Bhargava, B. L.; Balasubramanian, S. *J. Am. Chem. Soc.* **2006**, *128*, 10073.
(14) Gannon, T. J.; Law, G.; Watson, P. R. *Langmuir* **1999**, *15*, 8429.
(15) Law, G.; Watson, P. R. *Langmuir* **2001**, *17*, 6138.
(16) Law, G.; Watson, P. R. *Chem. Phys. Lett.* **2001**, *345*, 1.
(17) Law, G.; Watson, P. R.; Carmichael, A. J.; Seddon, K. R. *Phys. Chem. Chem. Phys.* **2001**, *3*, 2879.
(18) Baldelli, S. J. *J. Phys. Chem. B* **2003**, *107*, 6148.
(19) Fletcher, K. A.; Pandey, S. *Langmuir* **2004**, *20*, 33.
(20) Rivera-Ruberto, S.; Baldelli, S. *J. Am. Chem. Soc.* **2004**, *126*, 11788.
(21) Bowers, J.; Vergara-Gutierrez, M. C. *Langmuir* **2004**, *20*, 309.
(22) Limori, T.; Iwahashi, T.; Ishii, H.; Seki, K.; Ouchi, Y.; Ozawa, R.; Hamahuchi, H.; Kim, D. *Chem. Phys. Lett.* **2004**, *389*, 321.
(23) Solutskin, E.; Ocko, B. M.; Taman, L.; Kuzmenko, I.; Gog, T.; Deutsch, M. *J. Am. Chem. Soc.* **2005**, *127*, 7796.
(24) Halka, V.; Tsekov, R.; Freyland, W. *Phys. Chem. Chem. Phys.* **2005**, *7*, 2038.
(25) Halka, V.; Tsekov, R.; Freyland, W. *J. Phys.: Condens. Matter* **2005**, *17*, S3325.
(26) Izvekov, S.; Voth, G. A. *J. Phys. Chem. B.* **2005**, *109*, 2469.
(27) Wang, Y.; Izvekov, S.; Yan, T.; Voth, G. A. *J. Phys. Chem. B* **2005**, *110*, 3564.
(28) Izvekov, S.; Voth, G. A. *J. Chem. Phys.* **2005**, *123*, 134105.
(29) Yan, T.; Burnham, C. J.; Del Popolo, M. G.; Voth, G. A. *J. Phys. Chem. B.* **2004**, *108*, 11877.
(30) Yan, T.; Wang, Y. T.; Gao, X. P.; Voth, G. A. To be submitted for publication.
(31) Wang, Y.; Voth, G. A. *J. Am. Chem. Soc.* **2005**, *127*, 12192.
(32) Hanke, C. G.; Prices, S. L.; Lynden-Bell, R. M. *Mol. Phys.* **2001**, *99*, 801.
(33) Margulis, C. J.; Stern, H. A.; Berne, B. J. *J. Phys. Chem.* **2002**, *106*, 12017.
(34) Del Popolo, M. G.; Voth, G. A. *J. Phys. Chem.* **2004**, *108*, 1744.
(35) Urahata, S. M.; Ribeiro, M. C. C. *J. Chem. Phys.* **2004**, *120*, 1855.
(36) Hardacre, C.; Holbrey, J. D.; Jane, M. S. E.; Bowron, D. T.; Soper, A. K. *J. Chem. Phys.* **2003**, *118*, 273.
(37) Hardacre, C.; Jane, M., S. E.; Nieuwenhuyzen, M.; Bowron, D. T.; Soper, A. K. *J. Phys.: Condens. Matter* **2003**, *15*, S159.
(38) Car, R.; Parrinello, M. *Phys. Rev. Lett.* **1985**, *55*, 2471.
(39) Sprik, M. *J. Phys. Chem.* **1991**, *95*, 2283.
(40) Cornell, W. D.; Cieplak, P.; Bayly, C. I.; Gould, I. R.; Merz, K. M.; Ferguson, D. M.; Spellmeyer, D. C.; Fox, T.; Caldwell, J. W.; Kollman, P. A. *J. Am. Chem. Soc.* **1995**, *117*, 5179.
(41) Wang, Y.; Jiang, W.; Voth, G. A. Spatial heterogeneity in ionic liquids. In *Ionic Liquids IV: Not Just Solvents Anymore*; Brennecke, J. F., Rogers, R. D., Seddon, K. R., Eds.; ACS Symposium Series 975; American Chemical Society: Washington, DC, 2007; pp 272−307.
(42) Frisch, M. J.; Trucks, G. W.; Schlegel, H. B.; Scuseria, G. E.; Robb, M. A.; Cheeseman, J. R.; Montgomery, J. A., Jr.; Vreven, T.; Kudin, K. N.; Burant, J. C.; Millam, J. M.; Iyengar, S. S.; Tomasi, J.; Barone, V.; Mennucci, B.; Cossi, M.; Scalmani, G.; Rega, N.; Peterson, G. A.; Nakatsuji, H.; Hada, M.; Ehara, M.; Toyota, K.; Fukuda, R.; Hasegawa, J.; Ishida, M.; Nakajima, T.; Honda, Y.; Kitao, O.; Nakai, H.; Klene, M.; Li, X.; Knox, J. E.; Hratchian, H. P.; Cross, J. B.; Bakken, V.; Adamo, C.; Jaramillo, J.; Gomperts, R.; Stratmann, R. E.; Yazyev, O.; Austin, A. J.; Cammi, R.; Pomelli, C.; Ochterski, J. W.; Ayala, P. Y.; Morokuma, K.; Voth, G. A.; Salvador, P.; Dannenberg, J. J.; Zakrzewski, V. G.; Dapprich, S.; Daniels, A. D.; Strain, M. C.; Farkas, O.; Malick, D. K.; Rabuck, A. D.; Raghavachari, K.; Foresman, J. B.; Ortiz, J. V.; Cui, Q.; Baboul, A. G.; Clifford, S.; Cioslowski, J.; Stefanov, B. B.; Liu, G.; Liashenko, A.; Piskorz, P.; Komaromi, I.; Martin, R. L.; Fox, D. J.; Keith, T.; Al-Laham, M. A.; Peng, C. Y.; Nanayakkara, A.; Challacombe, M.; Gill, P. M. W.; Johnson, B.; Chen, W.; Wong, M. W.; Gonzalez, C.; Pople, J. A. *Gaussian 03*; Gaussian, Inc.: Wallingford, CT, 2004.
(43) Melchionna, S.; Ciccotti, G.; Holian, B. L. *Mol. Phys.* **1993**, *78*, 533.
(44) Hoover, W. G. *Phys. Rev. A* **1985**, *31*, 1695.
(45) Canongia Lopes, J. N.; Padua, A. A. H. *J. Phys. Chem. B* **2006**, *110*, 3330.
(46) Morrow, T. I.; Maginn, E. J. *J. Phys. Chem.* **2002**, *106*, 12807.
(47) Cadera, C.; Anthony, J. L.; Shah, J. K.; Morrow, T. I.; Brennecke, J. F.; Maginn, E. J. *J. Am. Chem. Soc.* **2004**, *126*, 5300.
(48) Cadena, C.; Maginn, E. J. *J. Phys. Chem.* **2006**, *110*, 18026.
(49) Langmuir, I. *Colloid Symp. Monogr.* **1925**, 48.
(50) Mach, P.; Huang, C. C.; Stoebe, T.; Wedell, E. D.; Nguyen, T.; Jeu, W. H. D.; Guittard, F.; Naciri, J.; Shashidhar, R.; Clark, N.; Jiang, I. M.; Kao, F. J.; Liu, H.; Nohira, H. *Langmuir* **1998**, *14*, 4330.